First measurement of $\pi^- e \to \pi^- e \gamma$ pion virtual compton scattering

A. Ocherashvili,[12,*] G. Alkhazov,[11] A. G. Atamantchouk,[11] M. Y. Balatz,[8,†] N. F. Bondar,[11] P. S. Cooper,[5] L. J. Dauwe,[17] G. V. Davidenko,[8] U. Dersch[9,‡] A. G. Dolgolenko,[8] G. B. Dzyubenko,[8] R. Edelstein,[3] L. Emediato,[19] A. M. F. Endler,[4] J. Engelfried,[13,5] I. Eschrich[9,§] C. O. Escobar,[19,‖] A. V. Evdokimov,[8] I. S. Filimonov[10,*] F. G. Garcia,[19,5] M. Gaspero,[18] I. Giller,[12] V. L. Golovtsov,[11] P. Gouffon,[19] E. Gülmez,[2] He Kangling,[7] M. Iori,[18] S. Y. Jun,[3] M. Kaya,[16] J. Kilmer,[5] V. T. Kim,[11] L. M. Kochenda,[11] I. Konorov,[9,¶] A. P. Kozhevnikov,[6] A. G. Krivshich,[11] H. Krüger,[9,**] M. A. Kubantsev,[8] V. P. Kubarovsky,[6] A. I. Kulyavtsev,[3,††] N. P. Kuropatkin,[11] V. F. Kurshetsov,[6] A. Kushnirenko,[3] S. Kwan,[5] J. Lach,[5] A. Lamberto,[20] L. G. Landsberg,[6] I. Larin,[8] E. M. Leikin,[10] Li Yunshan,[7] M. Luksys,[14] T. Lungov,[19,‡‡] V. P. Maleev,[11] D. Mao,[3,††] Mao Chensheng,[7] Mao Zhenlin,[7] P. Mathew,[3,§§] M. Mattson,[3] V. Matveev,[8] E. McCliment,[16] M. A. Moinester,[12] V. V. Molchanov,[6] A. Morelos,[13] K. D. Nelson,[16,‖‖] A. V. Nemitkin,[10] P. V. Neoustroev,[11] C. Newsom,[16] A. P. Nilov,[8] S. B. Nurushev,[6] A. Ocherashvili,[12] Y. Onel,[16] E. Ozel,[16] S. Ozkorucuklu,[16] A. Penzo,[20] S. I. Petrenko,[6] P. Pogodin,[16] B. Pouh,[9] M. Procario,[3,¶¶] V. A. Prutskoi,[8] E. Ramberg,[5] G. F. Rappazzo,[20] B. V. Razmyslovich,[11] V. I. Rud,[10] J. Russ,[3] P. Schiavon,[20] J. Simon,[9,***] A. I. Sitnikov,[8] D. Skow,[5] V. J. Smith,[15] M. Srivastava,[19] V. Steiner,[12] V. Stepanov,[11] L. Stutte,[5] M. Svoiski,[11] N. K. Terentyev,[11,3] G. P. Thomas,[1] L. N. Uvarov,[11] A. N. Vasiliev,[6] D. V. Vavilov,[6] V. S. Verebryusov,[8] V. A. Victorov,[6] V. E. Vishnyakov,[8] A. A. Vorobyov,[11] K. Vorwalter,[9,†††] J. You,[3,5] Zhao Wenheng,[7] Zheng Shuchen,[7] and R. Zukanovich-Funchal[19]

[1]*Ball State University, Muncie, Indiana 47306*
[2]*Bogazici University, Bebek, 80815 Istanbul, Turkey*
[3]*Carnegie-Mellon University, Pittsburgh, Pennsylvania 15213*
[4]*Centro Brasiliero de Pesquisas Físicas, Rio de Janeiro, Brazil*
[5]*Fermilab, Batavia, Illinois 60510*
[6]*Institute for High Energy Physics, Protvino, Russia*
[7]*Institute of High Energy Physics, Beijing, People's Republic of China*
[8]*Institute of Theoretical and Experimental Physics, Moscow, Russia*
[9]*Max-Planck-Institut für Kernphysik, D-69117 Heidelberg, Germany*
[10]*Moscow State University, Moscow, Russia*
[11]*Petersburg Nuclear Physics Institute, St. Petersburg, Russia*
[12]*Tel Aviv University, IL-69978 Ramat Aviv, Israel*
[13]*Universidad Autónoma de San Luis Potosí, San Luis Potosí, Mexico*
[14]*Universidade Federal da Paraíba, Paraíba, Brazil*
[15]*University of Bristol, Bristol BS8 1TL, United Kingdom*
[16]*University of Iowa, Iowa City, Iowa 52242*
[17]*University of Michigan-Flint, Flint, Michigan 48502*
[18]*University of Rome "La Sapienza" and INFN, Rome, Italy*
[19]*University of São Paulo, São Paulo, Brazil*
[20]*University of Trieste and INFN, Trieste, Italy*

(Received 9 September 2001; revised manuscript received 21 June 2002; published 26 September 2002)

Pion virtual compton scattering (VCS) via the reaction $\pi^- e \to \pi^- e \gamma$ was observed in the Fermilab E781 SELEX experiment. SELEX used a 600 GeV/c π^- beam incident on target atomic electrons, detecting the incident π^- and the final state π^-, electron and γ. Theoretical predictions based on chiral perturbation theory are incorporated into a Monte Carlo simulation of the experiment and are compared to the data. The number of reconstructed events ($=9$) and their distribution with respect to the kinematic variables (for the kinematic region studied) are in reasonable accord with the predictions. The corresponding π^- VCS experimental cross section is $\sigma = 38.8 \pm 13$ nb, in agreement with the theoretical expectation of $\sigma = 34.7$ nb.

DOI: 10.1103/PhysRevC.66.034613 PACS number(s): 13.60.Fz, 14.40.Aq

*Present address: Medson Ltd., Rehovot 76702, Israel.
†Deceased.
‡Present address: Infineon Technologies AG, München, Germany.
§Present address: Imperial College, London SW7 2BZ, U.K.
‖Present address: Instituto de Física da Universidade Estadual de Campinas, UNICAMP, SP, Brazil.
¶Present address: Physik-Department, Technische Universität München, 85748 Garching, Germany.
**Present address: The Boston Consulting Group, München, Germany.
††Present address: Fermilab, Batavia, IL.
‡‡Present address: Instituto de Física Teórica da Universidade Estadual Paulista, São Paulo, Brazil.
§§Present address: SPSS Inc., Chicago, IL.
‖‖Present address: University of Alabama at Birmingham, Birmingham, AL 35294.
¶¶Present address: DOE, Germantown, MD.
***Present address: Siemens Medizintechnik, Erlangen, Germany.
†††Present address: Deutsche Bank AG, Eschborn, Germany.

I. INTRODUCTION

The electric ($\overline{\alpha}$) and magnetic ($\overline{\beta}$) pion polarizabilities characterize the pion's deformation in an electromagnetic field, as occurs during $\gamma\pi$ Compton scattering. They depend on the rigidity of the pion's internal structure as a composite particle, and are therefore important dynamical quantities to test the validity of theoretical models. Based on chiral QCD, the chiral perturbation theory effective Lagrangian, using data from radiative pion β decay, predicts the pion electric and magnetic polarizabilities $\overline{\alpha}_\pi = -\overline{\beta}_\pi = 2.7 \pm 0.4$, expressed in units of 10^{-43} cm^3 [1–3]. Other theoretical predictions are also available [1].

The pion polarizabilities are usually investigated via their effect on the shape of the measured $\gamma\pi \to \gamma\pi$ real Compton scattering (RCS) angular distribution, as in Ref. [4]. Since pion targets are unavailable, pion RCS is approximated using different artifices (as shown in Fig. 1) such as the $\pi^- Z \to \pi^- Z\gamma$ Primakoff [5] and $\gamma p \to \gamma\pi^+ n$ radiative pion photoproduction reactions [6]; or by the crossing symmetry $\gamma\gamma \to \pi^+\pi^-$ two-photon reaction [2,7]. In the Primakoff scattering, a high-energy pion scatters from a (virtual, practically real) photon in the Coulomb field of the target nucleus. Values of $\overline{\alpha}$ measured by these experiments are given in Table I. They cover a large range of values and have large uncertainties. New high-precision pion polarizability measurements are therefore needed. Electromagnetic studies with virtual photons have the advantage that the energy and three-momentum of the virtual photon can be varied independently. In the pion $\gamma^*\pi \to \gamma\pi$ virtual Compton scattering (VCS) reaction, where the initial-state photon is virtual (far from the quasireal photons of Primakoff scattering) and the final-state photon is real, polarizabilities can be measured in the spacelike region, inaccessible by RCS [8]. We thereby access the so-called electric $\overline{\alpha}(q^2)$ and magnetic $\overline{\beta}(q^2)$ generalized polarizabilities of the pion [9], where $\overline{\alpha}(0)$ and $\overline{\beta}(0)$ correspond to the RCS $\overline{\alpha}$ and $\overline{\beta}$ pion Compton polarizabilities. The q^2-dependent $\overline{\alpha}(q^2)$ determines the change $\Delta F(q^2)$ in the pion charge form factor $F(q^2)$ in the presence of a strong electric field. The Fourier transform of $\overline{\alpha}(q^2)$ provides a picture of the local induced pion charge polarization density [10]. Similarly, first experiments [11] and calculations [12] have been carried out for proton VCS via $ep \to ep\gamma$.

We study experimentally the feasibility of extracting the "pion VCS" reaction

$$\pi^- e \to \pi^- e \gamma, \tag{1}$$

as a step in developing pion VCS as a new experimental tool for pion polarizability measurements. The data were taken with the Fermilab E781 SELEX spectrometer [13]. We used a 600 GeV/c π^- beam incident on target atomic electrons, detecting the incident π^- and the final state π^-, electron and γ. Theoretical predictions [14,15] based on chiral perturbation theory are incorporated into a Monte Carlo simulation of the experiment, and are compared to the data. With this theory, we calculated the total cross section (as described later) of the Eq. (1) process for a limited kinematic region discussed later [Eq. (6)], using the Monte Carlo integration program VEGAS [16]. The result is $\sigma(\text{total}) = 34.7 \pm 0.1$ nb. For the kinematic range considered, the integrated cross sections are not sensitive to the polarizabilities. We nonetheless chose this region in order to obtain sufficient statistics for a first study of the reaction.

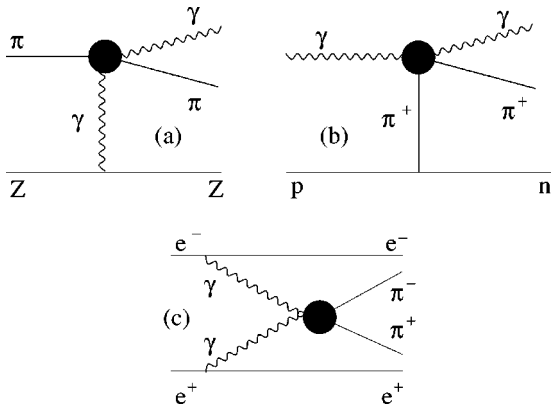

FIG. 1. Three-pion Compton scattering reactions. (a) $\pi^- Z \to \pi^- Z\gamma$, (b) $\gamma p \to \gamma\pi^+ n$, and (c) $e^+e^- \to e^+e^-\pi^-\pi^+$.

II. VCS KINEMATICS AND THEORETICAL DIFFERENTIAL CROSS SECTION

We study reaction (1) in terms of the following five independent invariant variables:

$$\begin{aligned} s &= (p_i + k)^2, \\ s_1 &= (k' + q')^2, \quad s_2 = (p_f + q')^2, \\ r^2 &= (p_i - p_f)^2, \quad q^2 = (k' - k)^2. \end{aligned} \tag{2}$$

Here p_i is the four-momentum of the incoming pion, k is the four-momentum of the target electron, and p_f, k', q' are the four-momenta of the outgoing pion, electron, and photon, respectively, as shown in Fig. 2. The differential cross section of reaction (1) in the convention of Ref. [17] reads as

$$d\sigma = \frac{m_e^2}{8E_f E_{k'} E_{q'}} \frac{1}{\sqrt{(p_i \cdot k)^2 - M_\pi^2 m_e^2}} \frac{1}{(2\pi)^5} \cdot |\overline{\mathcal{M}}|^2 \delta^4(p_i + k - p_f - k' - q') d^3p_f d^3k' d^3q'. \tag{3}$$

The invariant amplitude $\mathcal{M}$ contains the complete information on the dynamics of the process. The quantity $|\overline{\mathcal{M}}|^2$ indicates the sum over the final states and the average over the

TABLE I. Experimental values of $\overline{\alpha}$.

Reaction	$\overline{\alpha}$ [10^{-43} cm^3]	Reference
$\pi^- Z \to \pi^- Z\gamma$	$6.8 \pm 1.4 \pm 1.2$	[5]
$\gamma p \to \gamma\pi^+ n$	20 ± 12	[6]
$\gamma\gamma \to \pi^+\pi^-$	2.2 ± 1.6	[2,7]

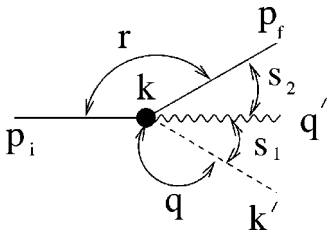

FIG. 2. Kinematics of the Eq. (1) reaction in the laboratory frame. The incoming pion beam with four-momentum p_i interacts with the target electron with four-momentum k and produces the outgoing pion with four-momentum p_f, γ with four-momentum q', and electron with four-momentum k'.

initial spin states. The fourfold differential cross section in terms of independent invariant variables of Eq. (2) involves a kinematical function λ [18] and a Jacobian matrix Δ_4 defining the phase space of the physical areas, and is given by

$$\frac{d\sigma}{ds_1 ds_2 dq^2 dr^2} = \frac{1}{(2\pi)^5} \frac{2m_e^2}{\lambda(s,m_e^2,m_\pi^2)} \frac{\pi}{16} \frac{1}{(-\Delta_4)^{1/2}} |\overline{\mathcal{M}}|^2. \tag{4}$$

Since the variable s, involving the energies of the beam pion and of the target electron, is fixed; the differential cross section (4) actually depends on four variables.

In reaction (1), the final photon can be emitted either by the electron or by the pion, as shown in Fig. 3. The first process is described by the Bethe-Heitler (BH) amplitude [Figs. 3(a) and 3(b)], calculable from quantum electrodynamics. The second process is described by the VCS [Fig. 3(c)] amplitude. Since the source of the final photon emission is indistinguishable, one obtains the following form of the matrix element of reaction (1) [14]:

$$\begin{aligned} |\overline{\mathcal{M}}|^2 &= \frac{1}{2} \sum (\mathcal{M}^{VCS} + \mathcal{M}^{BH})(\mathcal{M}^{VCS*} + \mathcal{M}^{BH*}) \\ &= |\overline{\mathcal{M}^{BH}}|^2 + |\overline{\mathcal{M}^{VCS}}|^2 \\ &\quad + |\overline{\mathcal{M}^{VCS}\mathcal{M}^{BH*} + \mathcal{M}^{VCS*}\mathcal{M}^{BH}}|, \end{aligned} \tag{5}$$

where $\mathcal{M}^{BH}$ and $\mathcal{M}^{VCS}$ are amplitudes of the BH and VCS processes.

The general features of the fourfold differential cross section can be inferred from Eq. (4) and matrix element calculations. The s_1 dependence is dominated by the $(s_1 - m_e^2)^{-1}$ pole of BH, the cross section varies accordingly, and is only slightly modified by the s_1 dependence of the VCS amplitude. The s_2 dependence is dominated by the $(s_2 - M_\pi^2)^{-1}$ pole of the VCS amplitude with modification of s_2 dependence of the BH amplitude, but in this case the modification is not as small as in the case of s_1. The r^2 dependence is determined by the r^{-4} pole of the BH amplitude, and the q^2 dependence follows the q^{-4} pole behavior of typical electron scattering. The energy of the outgoing pion is expected to be high while the angle is expected to be small according to the r^{-4} behavior of the cross section. The energy of the outgoing photon is mainly expected to be low,

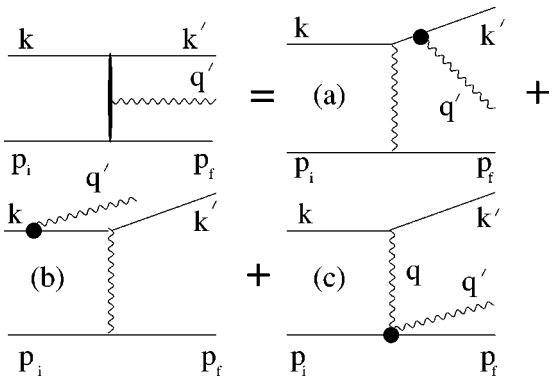

FIG. 3. The three Feynman diagrams corresponding to the $\pi^- e \to \pi^- e \gamma$. In the one-photon exchange approximation, (a) and (b) correspond to the BH process, while (c) corresponds to the VCS process. Here, q is the four-momentum of the virtual photon, $q = k' - k$.

as follows from the infrared divergence of the BH amplitude. The angular behavior of the outgoing photon is determined by the $(s_1 - m_e^2)^{-1}$ and $(s_2 - M_\pi^2)^{-1}$ poles of the BH and VCS amplitudes. The more interesting photons related to the generalized polarizabilities are expected to have higher energies. The behavior of the outgoing electron is completely determined by the q^{-4} behavior of the cross section.

III. EXPERIMENTAL APPARATUS AND TRIGGER

Our data were taken with the Hadron-Electron (HE) scattering trigger [19] of experiment E781/SELEX at Fermilab. SELEX uses a negatively charged beam of 600 GeV/c with full width momentum spread of $dp/p = \pm 8\%$, and an opening solid angle of 0.5 μsr. The beam consisted of approximately 50% π^- and 50% Σ^-. SELEX used copper and carbon targets, totaling 4.2% of an interaction length, with target electron thicknesses of 0.676 b^{-1} and 0.645 b^{-1}, respectively.

The experiment focused on charm baryon hadroproduction and spectroscopy at large x_F. The spectrometer hosted several projects that exploit physics with a small number of tracks compared to charm. SELEX had good efficiency for detecting all particles in the final state since the produced particles and decay fragments at large-x_F production are focused in a forward cone in the laboratory frame. Other requirements in the charm program for background suppression include good vertex resolution and particle identification over a large momentum range.

Four dipole magnets divide SELEX into independent spectrometers (beam, $M1$, $M2$, and $M3$), each dedicated to one special momentum region. Each spectrometer had a combination of tracking detectors. The $M1$, $M2$, and $M3$ spectrometers included electromagnetic calorimeters. The π-e separation for hadron-electron scattering used the $M2$ particle identification transition radiation detector and also the electromagnetic calorimeter.

The HE scattering trigger was specialized for separation of hadron-electron elastic scattering events. The trigger used information from a charged particle detector just downstream

of the target and, from a hodoscope just downstream of $M2$, to determine charged particle multiplicity and charge polarity. For the HE requirement, no electromagnetic calorimeter information was included. Therefore, the data collected via this trigger included hadron-electron elastic and inelastic scattering events.

IV. MONTE CARLO SIMULATION

Monte Carlo simulations were carried out for π^- VCS signal (1) and background event distributions with respect to the four invariants s_1, s_2, q^2, and r^2. We used the SELEX GEANT package GE781 [20]. The Monte Carlo (MC) study was carried out in the following four steps:

(1) A VCS event generator was written to search for the regions of phase space where the data are sensitive to pion structure. Several event generators were made to simulate a variety of expected backgrounds.

(2) The event generators were implemented into the simulation package. We studied the resolution, detection efficiency, and geometric and trigger acceptances for the signal and the background.

(3) The offline analysis procedure was developed and tuned to devise software cuts eliminating background while preserving a VCS signal.

(4) Finally, we estimated the expected number of π^- VCS events.

The VCS event generator is written, based on differential cross section (4), matrix element calculations, and three-body final-state kinematics. The acceptance-rejection method [21] is used for event generation. The VCS cross section increases rapidly when the direction of the outgoing real photon is close to the direction of one of the outgoing charged particles [due to the $(s_1-m_e^2)^{-1}$ pole of BH and the $(s_2-M_\pi^2)^{-1}$ pole of VCS], or when the energy of the outgoing real photon comes close to zero [due to the infrared divergence of the BH $(s_1-m_e^2-q^2+r^2)^{-1}$ pole]. Therefore, if events are generated in the pole region, then the efficiency of the acceptance-rejection method can be rather low, for the more interesting nonpole regions. In order to generate events at an acceptable rate, the pole regions are eliminated. Invariants are generated in the following regions:

$$1000m_e^2 \leqslant s_1 \leqslant M_\rho^2,$$

$$2M_\pi^2 \leqslant s_2 \leqslant M_\rho^2,$$

$$-0.2\ \mathrm{GeV}^2 < q^2 < -0.032\ \mathrm{GeV}^2,$$

$$-0.2\ \mathrm{GeV}^2 < r^2 < -2m_e E_\gamma(\min) + q^2 + s_1 - m_e^2. \quad (6)$$

For the photon minimum energy, we choose $E_\gamma(\min) = 5$ GeV to cut the infrared divergence of BH, and to be above the calorimeter noise. Since the VCS calculation does not explicitly include the ρ resonance, we choose upper limits of M_ρ^2 for s_1 and s_2. In Fig. 4, we show the generated distribution of events plotted with respect to the Mandelstam invariants, without correction for any acceptances. The solid and dashed curves are for BH+VCS and BH, respectively.

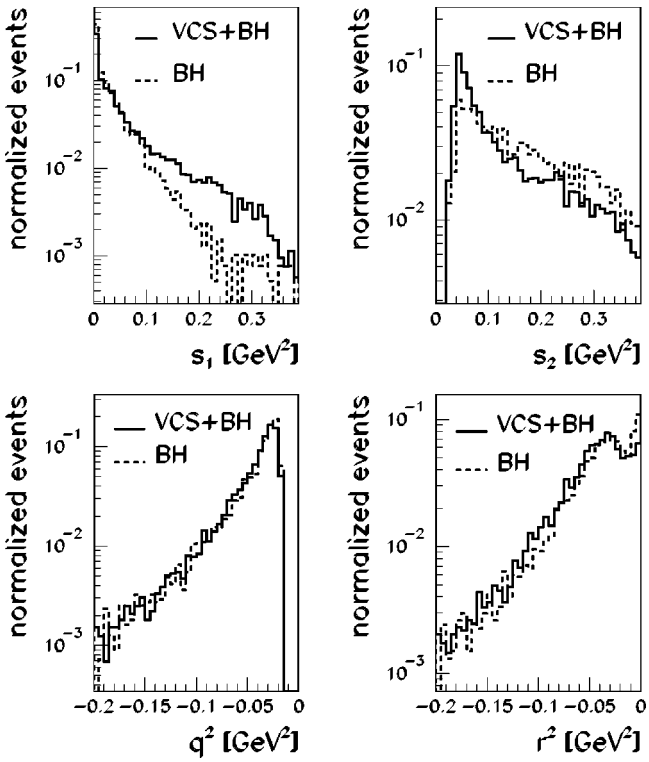

FIG. 4. Generated distributions of events plotted with respect to the Mandelstam invariants (solid line corresponds to the generation with full VCS amplitude and dashed line corresponds to the generation where only BH amplitude was used).

The VCS amplitude clearly affects the shape of these distributions for x_1 and s_2. For q^2 and r^2, the effect is difficult to see for the statistics shown. Taken together, the experiment therefore is potentially sensitive to the pion VCS amplitude. Since π/e separation is not 100% efficient, all interactions that produce two negatively charged tracks and a photon in the final state can generate the pattern of the pion VCS; i.e., can create background to the required measurement. For the background simulation, as well as in case of the VCS simulation, we require 5-GeV minimum energy for the photon.

The dominant background process for pion VCS is $\pi^- e$ elastic scattering followed by final-state interactions of the outgoing charged particles, such as the bremsstrahlung. The MC simulation shows that 28% of the original $\pi^- e$ elastic scattering events generate more than 5-GeV bremsstrahlung photons somewhere in the SELEX apparatus. We therefore consider the s_3 invariant mass of the outgoing $\pi^- e$ system:

$$s_3 = (p_f + k')^2. \quad (7)$$

We expect $s_3 = s$ for elastic scattering, and $s_3 = s_1 - s_2 + m_e^2 + M_\pi^2$ for VCS. Figure 5 shows generated and reconstructed elastic and VCS events subjected to the same charged particle track reconstruction and trigger requirements as the data. The data shown are only in the kinematic region of Eq. (6). As seen from Fig. 5, the events in the data at low s_3 do not arise from $\pi^- e$ elastic or π^- VCS. To describe the events with low s_3, we simulate backgrounds (with corrections for acceptances) from the interactions

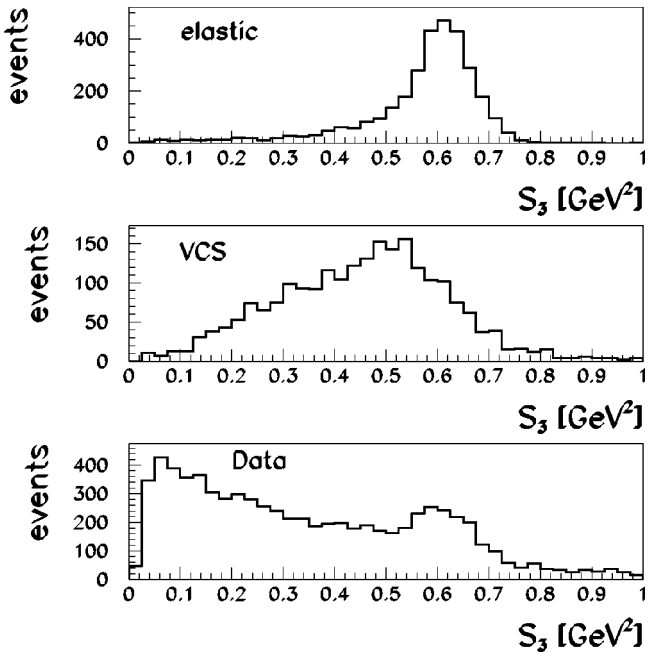

FIG. 5. Comparison of simulated s_3 distributions for $\pi^- e$ elastic scattering (top) and pion VCS (middle) with the data (bottom).

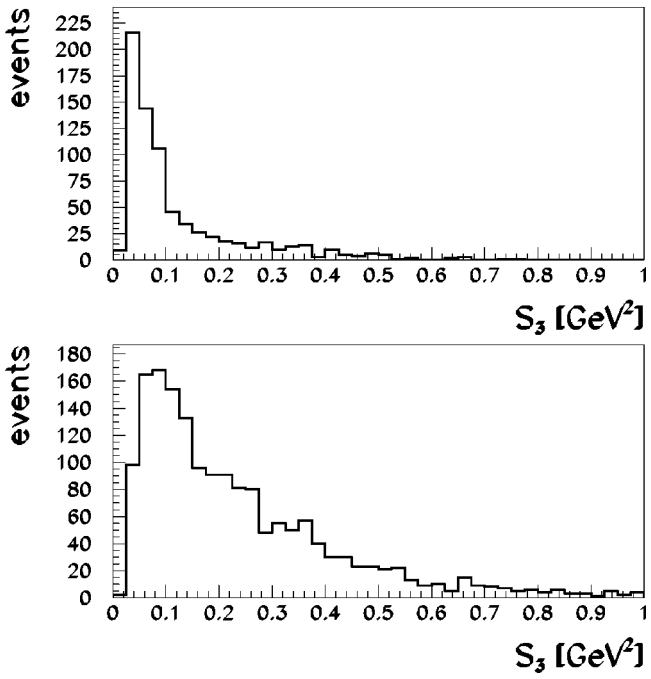

FIG. 6. Background via meson production; simulated s_3 distribution for $\pi^- e \to \rho e'$ (upper), and for $\pi^- A(Z) \to M A(Z)$ (lower), with arbitrary normalization.

$$\pi^- e \to M e, \tag{8}$$

$$\pi^- A(Z) \to M A(Z), \tag{9}$$

where M in Eqs. (8) and (9) is an intermediate meson state that can decay via $\pi^-\pi^0$, $\pi^-\eta$, $\pi^-\omega$, etc. Considering the threshold energies of reaction (8), only ρ meson production is allowed at SELEX energies. Figure 6 shows the simulated s_3 distributions for reactions (8) and (9), with the same acceptance requirements as in Fig. 5.

SELEX GE781 allows us to estimate the background rate from $\pi^- e$ elastic scattering. However, it is very difficult to estimate the background rate from all neutral meson (π^0, etc.) production reactions, such as those shown in Fig. 6. The data of Fig. 5 (bottom) are qualitatively well described by a combination of elastic (Fig. 5, top) and meson production (Fig. 6, bottom) channels. The contributions of VCS (Fig. 5, middle) and ρ production (Fig. 6, top) are relatively much lower. We do not show the quantitative sum of all contributions because of the difficulty to estimate the absolute yields of all meson production channels. Instead, we seek a set of cuts that remove as ''completely'' as possible the background from all γ sources, arising from neutral meson decays.

Since we measure all outgoing particles, the reaction kinematics are overdetermined. Therefore, in the data analysis, a constrained χ^2 fitting procedure [22] is used. A veto condition is used based on a two-body final-state constrained χ^2 kinematic fit for reduction of the background from $\pi^- e$ elastic scattering [23]. A three-body final-state constrained χ^2 kinematic fit is used for extracting the pion VCS signal.

A final-state electron can arise from photon conversion. For this background, the electron is not created at the same vertex as the pion. Consequently, the quality of the three-track vertex reconstruction should be low. Also, the simulation shows that no VCS outgoing particles hit the upstream photon calorimeter. Therefore, in addition to the constrained kinematic fitting cuts, we use restrictions on the vertex quality and on the total energy deposit in the upstream photon calorimeter to suppress backgrounds.

An additional way to reduce the background from $\pi^- e$ elastic scattering is to use the γe invariant mass s_1 and the Θ_{s_1} angle [angle between p_i and $(q'+k')$; see Fig. 2]. The simulation shows that if the final photon is emitted via electron bremsstrahlung, the value of s_1 should be low. On the other hand if the photon and electron are produced via π^0, η or ω meson, s_1 will ''remember'' the mass of the parent particle. Constraining the value of the s_1 invariant to be between the squared mass of π^0 and η mesons cuts the background from the electron bremsstrahlung and from the reaction (9). Figure 7 shows the distributions of VCS and background simulations. It is seen that the region with higher $\sqrt{s_1}$ and lower Θ_{s_1} are mostly populated with pion VCS. Another possibility to reduce the background from interactions (8–9) is to cut on the invariant M, defined as

$$M = \sqrt{(P_\pi + P_e - P_{e'})^2}. \tag{10}$$

For elastic events, $M = M_\pi$; for VCS, $M = \sqrt{s_2}$; and for ρ production, $M = M_\rho$ (see Fig. 8). The set of the final cuts is as follows:

(1) Fulfillment of the pion VCS pattern with identified electron; $E_\gamma \geqslant 5$ GeV for photons observed at laboratory angles less than 20 mrad in the downstream electromagnetic calorimeters; no additional tracks and vertices; and the total

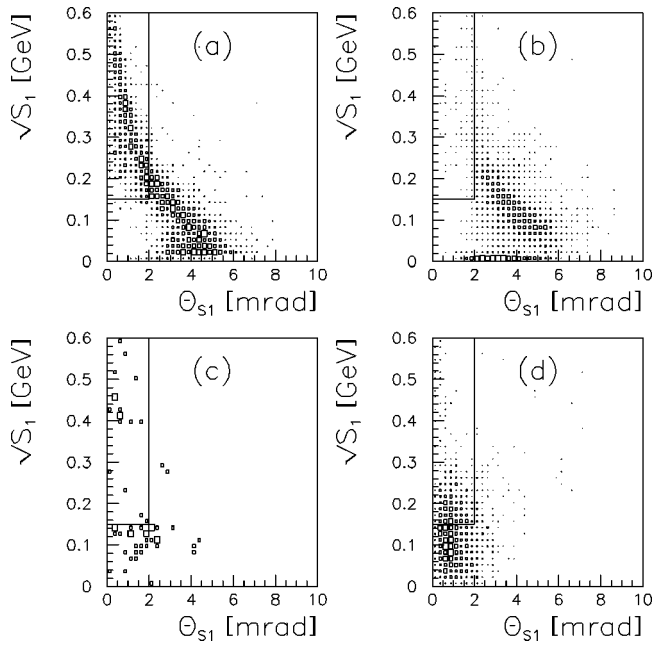

FIG. 7. $\sqrt{s_1}$, Θ_{s_1} correlation for (a) VCS, (b) $\pi^- e$ elastic scattering, (c) intermediate meson, and (d) ρ meson production. Only events inside the Θ_{s_1}-$\sqrt{s_1}$ region indicated by the box were accepted for further analysis.

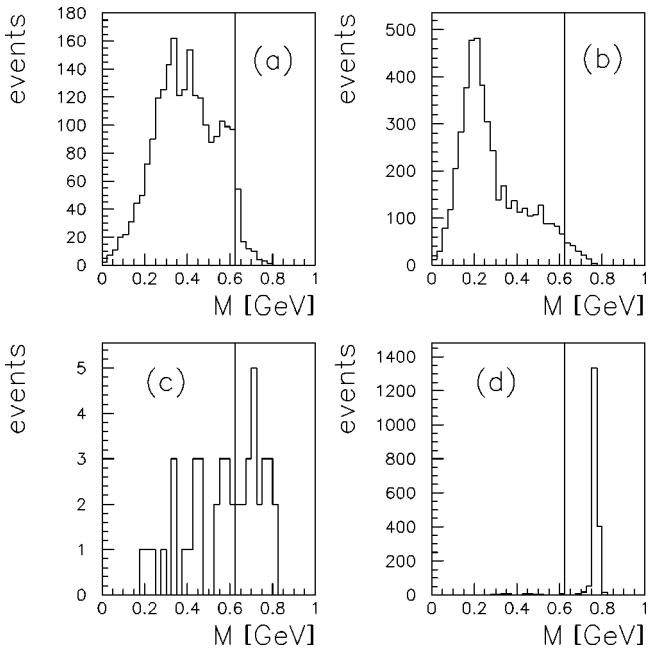

FIG. 8. Generated distribution of the M invariant for (a) VCS, (b) elastic scattering, (c) meson production reaction (9) and (d) ρ production reaction (8). The vertical lines show the 0.625-GeV M-cut position.

energy deposit is less than 1 GeV in the upstream electromagnetic calorimeter, covering detection angles greater than 30 mrad.

(2) Equation (6) ranges for the invariants, with $s_1(\min) = 0.0225\ \mathrm{GeV}^2$.

(3) $\chi^2_{elastic} > 20$, following a constrained fit procedure [22,23].

(4) $\chi^2_{VCS} \leqslant 5$, following a constrained fit procedure [22,14].

(5) $\Theta_{s_1} < 2$ mrad, $M \leqslant 0.625$ GeV.

To estimate the number of expected VCS events, as well as the yields of other $\pi^- e$ elastic or inelastic scattering events, we use

$$N_{\pi e} = N_\pi \sigma N_T \epsilon_{ex} \epsilon_r \,. \tag{11}$$

Here $N_{\pi e}$ is the number of events observed for a particular πe reaction, N_π is the number of incident beam pions ($\sim 4.4\times 10^{10}$ as measured by beam scalers and including particle identification), σ is the cross section for the particular reaction, ϵ_r is the offline reconstruction efficiency (36.6% for elastic and 2.65% for VCS) of the studied process, and N_T is the target electron density. Since not all experimental properties are implemented in GEANT, an additional efficiency factor ϵ_{ex} is included in Eq. (11). This efficiency factor is common to πe elastic and pion VCS reactions. The value ϵ_{ex} is calculated by comparison of the actual number of observed πe elastic scattering events to the expected number of events. The common efficiency arises since these two reactions have practically the same q^2 dependence; q^2 being the only kinematical parameter relevant for the trigger and first-order data reduction procedure. We calculate the experimental efficiency ϵ_{ex} (13.4%) from πe elastic scattering, as described in Ref. [14]. For extraction of the reference πe elastic scattering events, we employ the cuts of the SELEX πe elastic scattering analysis [23]. The cuts described above, considering the studied sources of background, improve the signal/noise ratio from less than 1/400 to more than 361/1. For these estimates, we used the following cross sections: $\sigma_{VCS} = 34.7$ nb and $\sigma_{elastic} = 4.27\ \mu$b for πe scattering; $\sigma_{Primakoff}(\mathrm{C\ target}) = 0.025$ mb and $\sigma_{Primakoff}(\mathrm{Cu\ target}) = 0.83$ mb for the Z^2-dependent Primakoff scattering. Based on the calculated pion VCS cross section, we expect around eight events in the π^- data sample.

The effect of the above enumerated cuts on the VCS signal and on the backgrounds coming from πe elastic scattering and Primakoff meson production, are listed in Table II. The results are based on the estimated relative cross section for these three processes [14]. The cuts are very effective in removing backgrounds while retaining signal events, such that the final event sample is essentially pure pion VCS.

V. DATA ANALYSIS

In the first-stage analysis, events containing one identified electron are selected. For these events, particle trajectories are checked if they form a vertex inside the target material. An event is accepted if it contains exactly three tracks, including the beam particle and an electron candidate, and forms one vertex in the target. We consider data only in the kinematic region of Eq. (6). On the accepted data set, we applied the system of the cuts discussed above. The working statistics with these cuts on the data are given in Table III and in Fig 9, where we show the effects of the cuts on the s_3

TABLE II. Percentages of the remaining events after using the cuts for the MC simulated π VCS and background events.

Cuts	VCS	Elastic	Meson production
1	29.8	32.1	0.24
2	9.97	9.21	0.03
3	8.89	0.03	0.03
4	3.58	0.003	0.004
5	2.56	<0.001	$<3.0\times10^{-6}$

invariant. The effect of the cuts on the data (Table III) is comparable to the effect on the simulated VCS events (Table II). Finally nine events (with a statistical uncertainty of ±3) were accepted as pion VCS. The corresponding π VCS experimental cross section based on Eq. (11) under the assumption that the background has been completely eliminated is $\sigma=38.8\pm13$ nb, in agreement with the theoretical expectation of $\sigma=34.7$ nb. The error given is only statistical, and does not include possible systematic uncertainties in the efficiency product $\epsilon_{ex}\epsilon_r$ in Eq. (11).

The comparisons of reconstructed (data) and generated (theory) event distributions, normalized to unit area, are shown in Fig. 10 with respect to the four invariants s_1, s_2, q^2, and r^2 of Eq. (2), and are shown with binning that matches the experimental resolutions. The resolution for each variable was found by Monte Carlo simulation, comparing reconstructed and generated events. To check whether the data and theory (MC) distributions are consistent with each other, we use the test of Kolmogorov and Smirnov (KS) [24]. The KS test is based on normalized cumulative distribution functions (CDFs). We use the KS D statistic, as a measure of the overall difference between the two CDFs. It is defined as the maximum value of the absolute difference between two CDFs. The significance level for a value D (as a disproof of the null hypothesis that the distributions are the same) is given by the probability $P(D)$ [24]. A high value of $P(D)$ means that the data and theory CDFs are consistent with one another.

Following the KS procedure, we calculate the normalized cumulative distributions of data and theory, corresponding to Figs. 10(a–d).The KS D statistic, and the KS probabilities for consistency of theory/data distributions, are given in Table IV and Figs. 11 and 12. The experimental and theoretical CDFs for s_1 and r^2 look similar. For s_2 and q^2, some regions of q^2 (s_2) have the experimental CDFs larger (smaller) than the theoretical CDFs. The values of $P(D)$ (see

TABLE III. Percentages of events remaining after using the cuts.

Cuts	Percentages of remaining events
1	26.8
2	13.9
3	9.93
4	0.61
5	0.13

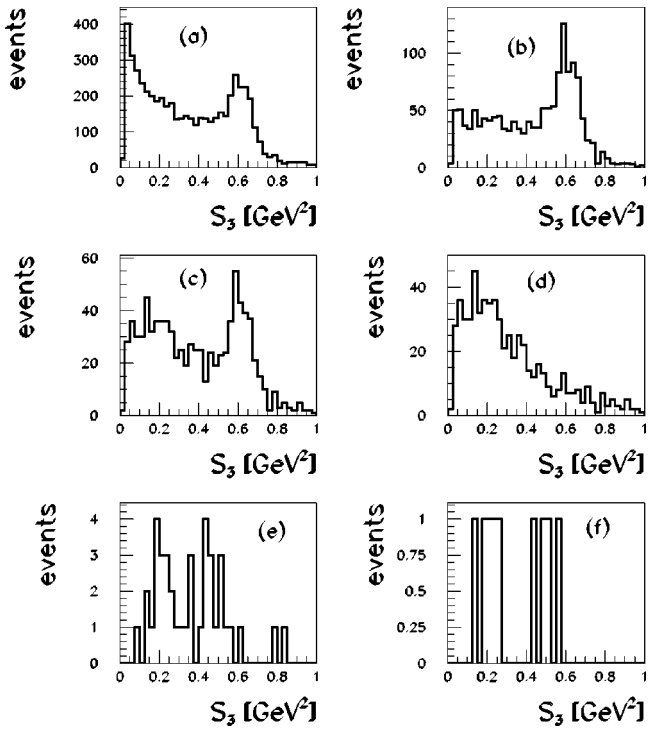

FIG. 9. Effect of the cuts on s_3 invariant; (a) raw distribution, (b) after cut 1, (c) after cut 2, (d) after cut 3, (e) after cut 4, and (f) final distribution of s_3 invariant.

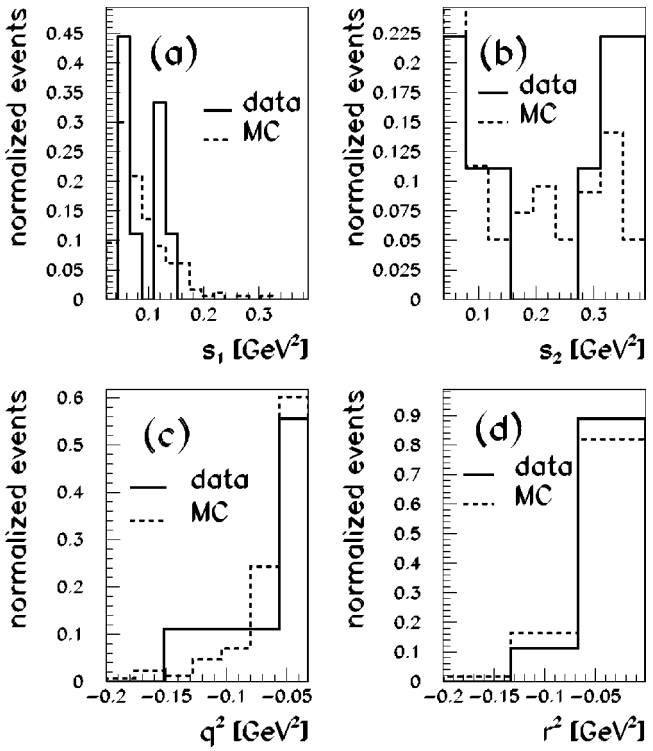

FIG. 10. Comparison of data and theory normalized distributions with respect to (a) s_1, (b) s_2, (c) q^2, and (d) r^2. The solid line corresponds to data and the dashed line corresponds to simulations with $\overline{\alpha}=2.7$. The simulation with $\overline{\alpha}=6.8$ gives practically the same result.

TABLE IV. Value of KS D statistic, and probabilities P, for comparison of data with theory for $\overline{\alpha}=2.7$. The comparison of data with theory for $\overline{\alpha}=6.8$ gives practically the same result.

Variable	D	$P(D)$
s_1	0.18	0.90
s_2	0.27	0.83
s_3	0.27	0.92
q^2	0.18	0.99
r^2	0.07	0.99

Table IV) are sufficiently high for all five CDFs, as expected if the experimental data are consistent with theory. In addition, the prediction of a total of eight events is in agreement with the observed 9 ± 3 data events. This further supports the conclusion from the KS test that we observe pion VCS events.

From the limited statistics and sensitivity of this first pion VCS experiment, we cannot determine the $\overline{\alpha}$ polarizability value, nor can we determine which value of $\overline{\alpha}$ is preferred. In a future experiment, the sensitivity to pion polarizability may be increased [14] by achieving a dataset in which the final $\gamma(\pi)$ has higher (lower) energies. However, such data correspond to a lower cross section, and therefore require a high luminosity experiment.

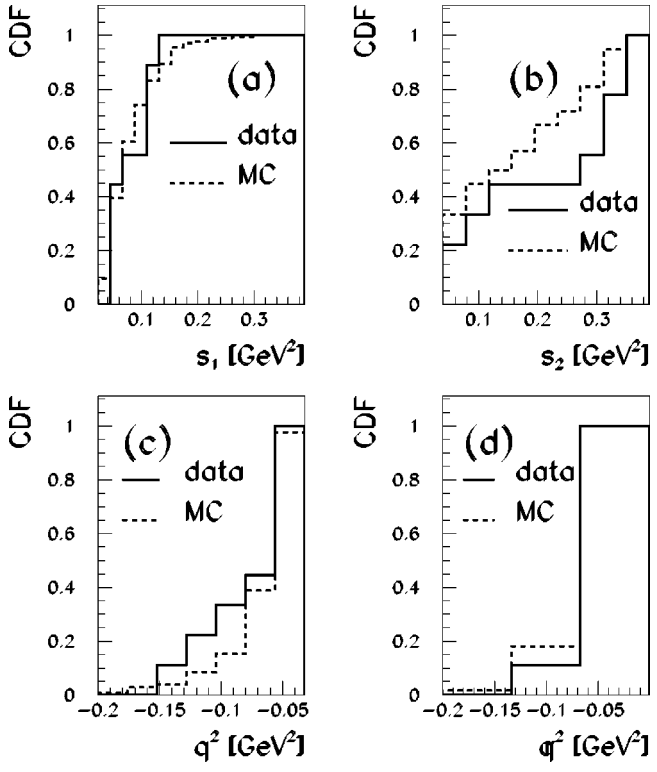

FIG. 11. Normalized cumulative distributions for data and theory versus (a) s_1, (b) s_2, (c) q^2, and (d) r^2 invariants. The solid line corresponds to data, the dashed line corresponds to MC theory simulations with $\overline{\alpha}=2.7$. The simulation with $\overline{\alpha}=6.8$ gives practically the same result.

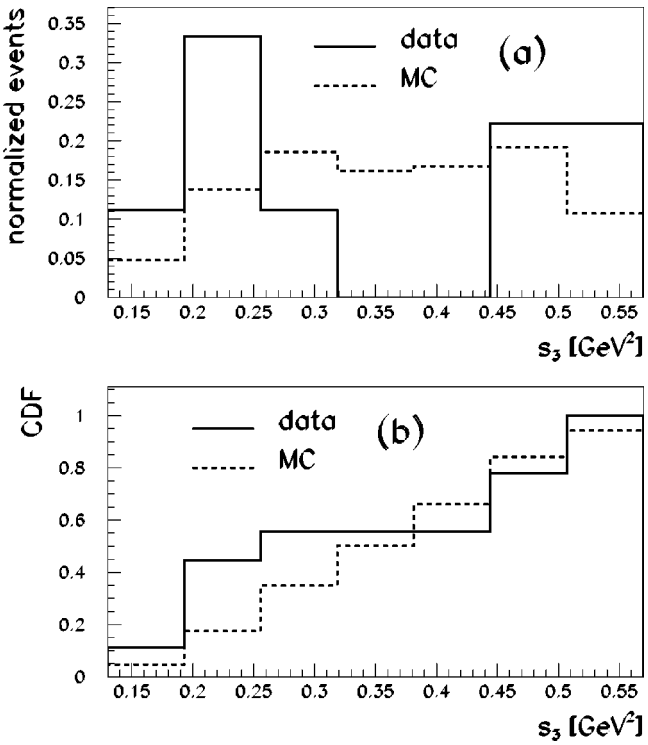

FIG. 12. Comparison of data and theory normalized distributions with respect to s_3 (a), and normalized cumulative distributions for data and theory versus s_3 (b). The solid line corresponds to data, the dashed line corresponds to MC theory simulations with $\overline{\alpha}=2.7$. The simulation with $\overline{\alpha}=6.8$ gives practically the same result.

VI. CONCLUSIONS

The pion virtual Compton scattering via the reaction $\pi e \rightarrow \pi' e' \gamma$ is observed. We developed and implemented a simulation with a VCS event generator. We defined cuts that allow background reduction and VCS signal extraction. The measured number of reconstructed pion VCS events, and their distributions with respect to the Mandelstam invariants, are in reasonable agreement with theoretical expectations. The corresponding π VCS experimental cross section is $\sigma=38.8\pm13$ nb, in agreement with the theoretical expectation of $\sigma=34.7$ nb.

ACKNOWLEDGMENTS

The authors are indebted to the staffs of Fermi National Accelerator Laboratory, the Max-Planck-Institut für Kernphysik, the Carnegie Mellon University, the Petersburg Nuclear Physics Institute, and the Tel Aviv University for invaluable technical support. We thank Dr. C. Unkmeir and Dr. S. Scherer for the VCS matrix element calculation. This project was supported in part by Bundesministerium für Bildung, Wissenschaft, Forschung und Technologie, Consejo Nacional de Ciencia y Tecnología (CONACyT), Conselho Nacional de Desenvolvimento Científico e Tecnológico, Fondo de Apoyo a la Investigación (UASLP), Fundação de Amparo à Pesquisa do Estado de São Paulo (FAPESP), the Israel Science Foundation, the Istituto Nazionale de Fisica Nucleare (INFN), the International Science Foundation

(ISF), the National Science Foundation (Grant No. 9602178), the NATO (Grant No. CR6.941058-1360/94), the Russian Academy of Science, the Russian Ministry of Science and Technology, the Turkish Scientific and Technological Research Board (TÜBİTAK), the US Department of Energy (Grant No. DE-FG02-91ER40664 and Contract No. DE-AC02-76CHO3000), and the US-Israel Binational Science Foundation (BSF).

[1] J. Portales and M.R. Pennington, hep-ph/9407295; D. Morgan and M.R. Pennington, Phys. Lett. B **272**, 134 (1991).
[2] D. Babusci, S. Bellucci, G. Giordano, G. Matone, A.M. Sandorfi, and M.A. Moinester, Phys. Lett. B **277**, 158 (1992).
[3] B.R. Holstein, Comments Nucl. Part. Phys. **19**, 221 (1990).
[4] A. Klein, Phys. Rev. **99**, 988 (1955); A.M. Baldin, Nucl. Phys. **18**, 310 (1960); V.A. Petrun'kin, Sov. JETP **40**, 1148 (1961).
[5] Yu.M. Antipov *et al.*, Phys. Lett. **121B**, 445 (1983); Z. Phys. C **26**, 495 (1985).
[6] T.A. Aibergenov, P.S. Baranov, O.D. Beznisko, S.N. Cherepniya, L.V. Filkov, A.A. Nafikov, A.I. Osadchii, V.G. Raevsky, L.N. Shtarkov, and E.I. Tamm, Czech. J. Phys., Sect. A **36**, 948 (1986).
[7] J. Boyer *et al.*, Phys. Rev. D **42**, 1350 (1990).
[8] S. Scherer, Few-Body Syst., Suppl. **11**, 327 (1999); Czech. J. Phys. **49**, 1307 (1999).
[9] C. Unkmeir, S. Scherer, A.I. L'vov, and D. Drechsel, Phys. Rev. D **61**, 034002 (2000).
[10] A.I. L'vov, S. Scherer, B. Pasquini, C. Unkmeir, and D. Drechsel, Phys. Rev. C **64**, 015203 (2001).
[11] S. Kerhoas *et al.*, Nucl. Phys. **A666-A667**, 44 (2000); J. Roche *et al.*, Phys. Rev. Lett. **85**, 708 (2000).
[12] B. Pasquini, S. Scherer, and D. Drechsel, Phys. Rev. C **63**, 025205 (2001); nucl-th/0105074, and references therein.
[13] J. Russ *et al.*, a proposal to construct SELEX, Proposal PE781, Fermilab, 1987, http://fn781a.fnal.gov/
[14] C. Unkmeir, A. Ocherashvili, T. Fuchs, M.A. Moinester, and S. Scherer, Phys. Rev. C **65**, 015201 (2002); A. Ocherashvili, Ph.D. thesis, Tel Aviv University, 2000, http://www-nuclear.tau.ac.il/~ aharon/phd.html
[15] C. Unkmeir, Ph.D. thesis, Johannes Gutenberg University, Mainz, 2000; T. Fuchs, B. Pasquini, C. Unkmeir, and S. Scherer, hep-ph/0010218.
[16] G.P. Lepage, J. Comput. Phys. **27**, 192 (1978).
[17] J.D. Bjorken and S. D. Drell, *Relativistic Quantum Mechanics* (McGraw-Hill, New York, 1964).
[18] E. Byckling and K. Kajantie, *Particle Kinematics State* (Wiley, New York, 1973), pp. 102–145.
[19] K. Vorwalter, Ph.D. thesis, MPI, Heidelberg, 1998; H. Krüger, Ph.D. thesis, MPI, Heidelberg, 1999.
[20] G. Davidenko *et al.*, in *Proceedings of the International Conference on Computing in High Energy Physics '95* (World Scientific, Singapore, 1996), edited by R. Shellard and T. Nguyen, p. 832; G. Dirkes, H. Krüger, N.P. Kuropatkin, and J. Simon, *Data and GE781 Comparison for Elastic Scattering Physics*, (MPI, Heidelberg, in press); V. Steiner (private communication); I. Giller, M.Sc. thesis, Tel Aviv University, 1999; I. Eschrich *et al.*, Phys. Lett. B **522**, 233 (2001).
[21] Particle Data Group, C. Caso *et al.*, Eur. Phys. J. C **3**, 1 (1998).
[22] S. Brandt, *Data Analysis: Statistical and Computational Methods for Scientists and Engineers* (Springer-Verlag, Berlin, 1998).
[23] J. Simon, Ph.D. thesis, MPI, Heidelberg, 2000; G. Dirkes, M.Sc. thesis, MPI, Heidelberg, 1999.
[24] W.H. Press, S.A. Teukolsky, W.T. Vetterling, and B.P. Flannery, *Numerical Recipes in FORTRAN: The Art of Scientific Computing*, 2nd ed. (Cambridge University, 1992), pp. 617–622.